ACS APPLIED MATERIALS & INTERFACES

www.acsami.org

Research Article

Tunnel-Structured ζ-V_2O_5 as a Redox-Active Insertion Host for Hybrid Capacitive Deionization

Nicholas I. Cool, Randall James, Parker Schofield, Joseph V. Handy, Mukul Bhatia, and Sarbajit Banerjee*

Cite This: *ACS Appl. Mater. Interfaces* 2023, 15, 1554−1562

Read Online

ACCESS | Metrics & More | Article Recommendations | Supporting Information

ABSTRACT: Much of the earth's water has a salt content that is too high for human consumption or agricultural use. Enhanced oil recovery operations generate massive volumes of produced water waste with a high mineral content that can substantially exacerbate water distress. Current deionization techniques such as reverse osmosis function by removing the water (majority phase) from the salt (minority phase) and are thus exceedingly energy-intensive. Furthermore, these methods are limited in their ability to selectively extract high-value ions from produced water waste and brine streams. Hybrid capacitive deionization holds promise for enabling both desalination and resource recovery. In this work, we demonstrate the construction of a hybrid capacitive deionization cell that makes use of tunnel-structured ζ-V_2O_5 as a redox-active positive electrode material. By augmenting surface adsorption with Faradaic insertion processes, a 50% improvement in the ion removal capacity for K and Li ions is obtained as compared to a capacitive high-surface-area carbon electrode. The extracted ions are accommodated in surface sites and interstitial sites within the one-dimensional tunnel framework of ζ-V_2O_5. The kinetics of ion removal depend on the free energy of hydration, which governs the ease of desolvation at the electrode/electrolyte interface. The overall ion removal capacity additionally depends on the solid-state diffusion coefficient. ζ-V_2O_5 positive electrodes show substantial selectivity for Li^+ removal from mixed flow streams and enrichment of the Li-ion concentration from produced water waste derived from the Permian Basin.

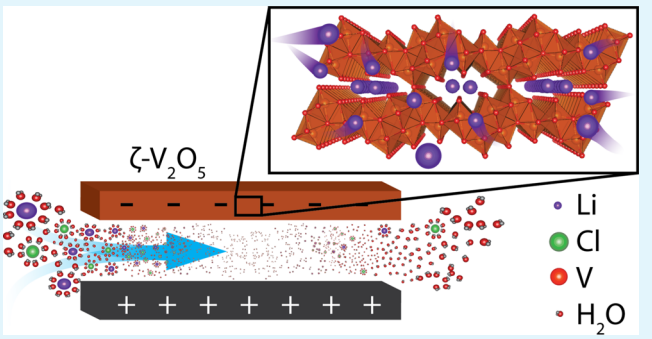

KEYWORDS: *desalination, hybrid capacitive deionization, ion capture, produced water, vanadium oxides, direct lithium extraction, resource recovery, metastable polymorphs*

INTRODUCTION

Fresh water is an increasingly valuable and scarce commodity across the world;[1] substantial recent efforts have focused on desalination of sea water, brackish water, and flowback and produced water (FPW) brought to the surface using hydraulic fracturing.[2−5] Despite notable advances in membrane design and process intensification, the majority of current desalination techniques such as reverse osmosis, multi-stage flash distillation, and direct solvent extraction require exceedingly high energy budgets.[6−9] In each of these techniques, the majority phase (water) is removed from the minority phase (dissolved salt ions), thereby requiring significant energy input to drive selective transport processes. Furthermore, these techniques are limited in their selectivity toward specific ions. Indeed, high-value ions such as lithium, rare-earth elements, and uranium are present in FPW in substantial quantities and are key to a new paradigm of resource recovery required for the energy transition.[10−12] FPW is currently viewed as a considerable environmental liability. Scanlon and co-workers estimate that in the Permian Basin spanning across Texas and New Mexico, FPW generated from conventional and unconventional reservoirs was as much as ca. 40×10^9 barrels and 4×10^9 barrels, respectively, between the years 2005 and 2015.[13] Owing to the high salinity of FPW and the complexity imbued by the presence of enhanced oil recovery additives, recovery and reuse of FPW are challenging, whereas reinjection into aquifers is subject to increasingly stringent regulations.[14] In contrast to traditional electrochemical desalination, which relies almost entirely on non-specific capacitive processes, hybrid capacitive desalination stores ions on surfaces through Faradaic pseudocapacitive processes and within the interior volumes of materials through redox reactions akin to those of positive electrode materials of Li-ion batteries.[15−17] Selectivity in ion extraction is engendered based on differences in insertion potentials, bulk diffusion coefficients, and interstitial

Received: October 2, 2022
Accepted: December 7, 2022
Published: December 21, 2022

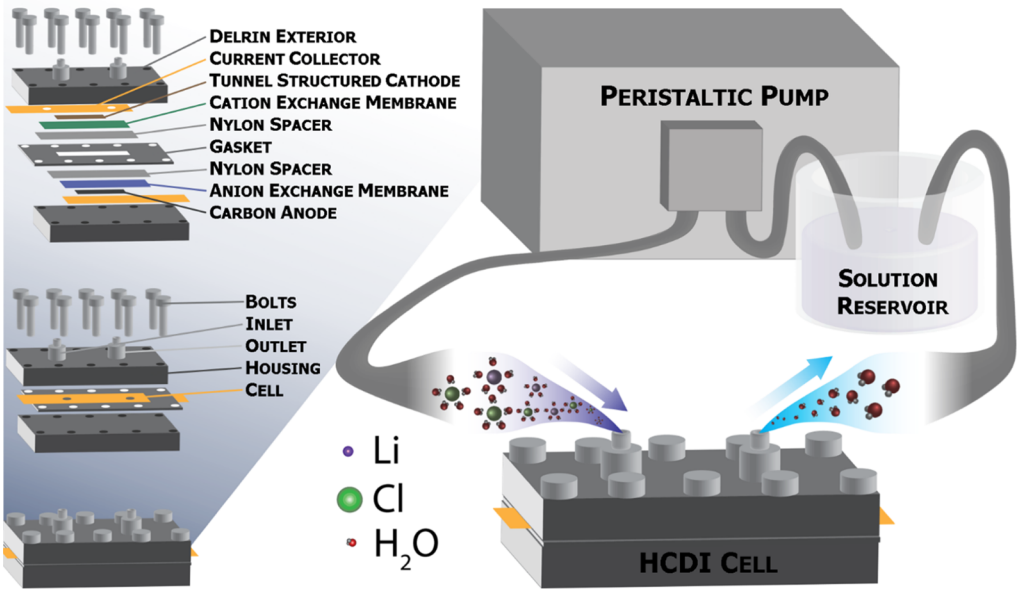

Figure 1. Components of the HCDI cell. Schematic illustration of the HCDI cell depicting the assembled components (left). Illustration of the HCDI cell connected to a peristaltic pump and solution reservoir (right).

site preferences of different ions. As such, hybrid capacitive deionization methods hold promise not just for enabling reuse of FPW in hydraulic fracturing operations but also for enabling the extraction of high-value ions.[18] In this article, we describe an electrochemical approach for desalination and selective ion capture based on sequestration of ions on surfaces and within the one-dimensional (1D) tunnels of ζ-V_2O_5, a versatile intercalation host for monovalent and multivalent ions.[19,20]

In conventional capacitive deionization (CDI) techniques, dissolved ions are removed from saline water by the application of a potential across a deionization cell comprising two high-surface-area carbon electrodes.[21−23] In this process, the dissolved ions migrate to electrified interfaces and constitute an electric double layer of solvated ions; the concentration of stored ions is directly proportional to the accessible surface area of the electrodes.[24−26] Several modifications have been implemented to increase the efficacy of CDI cells such as the implementation of electrodes with hierarchical porosity in order to increase the available surface area for ion adsorption and the addition of ion-exchange membranes that impede the diffusion of counter ions.[22,23,27,28] Although recent innovations have improved the capacity and efficiency of CDI cells, the fundamental drawback of this approach, which is that ion storage is limited to the electrical double layer formed on the wetted surfaces of the electrode material, remains a substantial constraint.[15]

Similar considerations related to surface versus bulk storage of ions represent a key difference in the operational mechanisms of supercapacitors and intercalation batteries. In positive electrodes of Li-ion or other intercalation batteries, ions are stored in interstitial sites within the bulk of the electrode materials based on concomitant redox reactions.[29] A key difference between hybrid CDI (HCDI) and CDI is the operation of Faradaic reactions in the former, which in addition to electric double layer formation result in interfacial desolvation and bulk diffusion of ions. Storing ions in interstitial sites, and not just within surface double layers, engenders a considerable increase in charge storage capacity.[24,30] A notable trade-off is that insertion electrodes can have a more sluggish rate of removal as a result of diffusion limitations and the operation of Faradaic processes at interfaces.[24,26,30] These limitations can be substantially alleviated through appropriate structuring of electrode tortuosity, control over crystallite dimensions, and modification of the structure and composition of the intercalation host. Insertion chemistry further provides a sensitive means of differentiating between uptake of different ions from aqueous media based on differentials in bulk diffusion coefficients and intercalation potentials, which, in turn, are governed by the crystal-lattice-dependent dimensions of interstitial sites, site-to-site migration barriers, and the thermodynamics of insertion reactions.[24,26,31]

ζ-V_2O_5, a 1D tunnel-structured polymorph of V_2O_5, is a promising candidate for use as a positive electrode material in HCDI owing to its high abundance of interstitial sites, accessibility of multi-electron redox on vanadium centers, low diffusion barriers for site-to-site ion migration, ability to insert a variety of cations, and excellent stability in aqueous media.[30,31] Indeed, ζ-V_2O_5 is one of many metastable polymorphs of V_2O_5 that has shown promise as a positive electrode material but is distinctive in its ability to accommodate both monovalent and multivalent cations, which is a result of a diverse range of variously coordinated interstitial sites arrayed along the edges and center of its 1D tunnel.[31] Furthermore, the high crustal abundance of vanadium (ca. 22 000 000 metric tons of known global reserves), a robust geographically dispersed supply chain, substantial recent advances in vanadium supply chains for co-production and primary production (over a 20% annual increase in projected supply), and an extensive recycling infrastructure make this element a viable electrode for desalination and lithium recovery at scale.[32,33] In this work, we demonstrate the construction and implementation of HCDI cells based on ζ-V_2O_5 active electrodes for sequestration of Li^+, Na^+, and K^+ ions from aqueous media. We demonstrate the intercalative and pseudocapacitive, and not just adsorptive, removal of cations by ζ-V_2O_5. Ion selectivity from mixed-ion streams is rationalized based on differences in

https://doi.org/10.1021/acsami.2c17800
ACS Appl. Mater. Interfaces 2023, 15, 1554−1562

the site preferences, hydration radius, and hydration free energy.

EXPERIMENTAL METHODS

Electrode Preparation. ζ-V_2O_5 was synthesized using a previously reported method.[19] In brief, silver acetate (0.2811 g) (Alfa Aesar) and α-V_2O_5 (0.9189 g) (EMD Millipore) were ball-milled for 30 min in a SPEX SamplePrep 5100 mixer mill using methacrylate grinding beads. Next, 0.33 g of the resulting mixture was added to 16 mL of deionized water (Barnstead International NANOpure Diamond system ρ = 18.2 MΩ·cm) and placed inside a polytetrafluoroethylene vessel, which was inserted into a Parr Instrument Company steel acid digestion vessel. The sealed hydrothermal vessel was heated at 210 °C for 72 h. Upon cooling the vessels to room temperature, the resulting green precipitate (β-$Ag_{0.33}V_2O_5$) was filtered and subsequently washed with copious amounts of water and 2-propanol. Resulting β-$Ag_{0.33}V_2O_5$ (0.33 g) was added to a polytetrafluoroethylene cup with 15 mL of deionized water (ρ = 18.2 MΩ·cm) and 0.8 mL of HCl (12 M) (Avantor) and again placed in a Parr Instrument Company steel acid digestion vessel. The hydrothermal vessel was heated at 210 °C for 24 h. Upon cooling the vessels to room temperature, the resulting brown precipitate (ζ-V_2O_5, AgCl) was filtered and subsequently washed with copious amounts of deionized water (ρ = 18.2 MΩ·cm) and 2-propanol. AgCl was then removed by treating the precipitate with 0.5 M $Na_2S_2O_3$ followed by washing with copious amounts of deionized water (ρ = 18.2 MΩ·cm).

The positive electrode material for HCDI cells was prepared by mixing 160 mg of the active material (ζ-V_2O_5), 30 mg of Super C45 conductive carbon black, and 1 mL of 10 wt. % poly(vinylidene difluoride) (PVDF) in *N*-methyl-2-pyrrolidone (NMP). The resulting slurry was stirred by hand for 30 min until an even viscous slurry was formed. The slurry was then cast onto battery-grade aluminum foil with a thickness of 15 μm using a BYK casting knife at a thickness of 0.25 mm. The cast electrodes were dried in a muffle furnace at 70 °C for 24 h. Individual electrodes were cut from the electrode material to form 1 cm × 4 cm electrodes each containing ca. 11 mg of the active material.

The negative electrode material for HCDI and both the negative and positive electrode materials for CDI cells were prepared by mixing 160 mg of the active material (Strem Chemicals activated carbon with a surface area of 1300−1400 m^2/g), 30 mg of Super C45 conductive carbon black, and 1 mL of 10 wt % PVDF in NMP. The resulting slurry was stirred by hand for 30 min until an even viscous slurry was formed. The slurry was then cast onto battery-grade aluminum foil with a thickness of 15 μm using a BYK casting knife at a thickness of 0.25 mm. The cast electrodes were dried in a muffle furnace at 70 °C for 24 h. Individual electrodes were cut from the electrode material to form 1 cm × 4 cm electrodes each containing 11 mg of the active material.

Cell Construction and Input Solutions. A custom HCDI cell was constructed using a Delrin exterior as sketched in Figure 1. The interior of the HCDI cell comprises a current collector (15.24 cm × 5.08 cm conductive copper tape), the positive electrode material (1 cm × 4 cm), a cation-exchange membrane (1.5 cm × 4.5 cm Nafion 115), two layers of a nylon separator material (78 μm × 100 μm pore size VWR), a custom Viton gasket (1/32 in McMaster-Carr), two layers of the separator (78 μm × 100 μm pore size VWR), an anion-exchange membrane (Fumasep FAA-3-PK-130), the negative electrode material, and a current collector (15.24 cm × 5.08 cm conductive copper tape). These components were then sandwiched between the Delrin exterior and connected to a peristaltic pump (Omega FPU 421). Various aqueous salt solutions containing 15.04 mm NaCl, LiCl, or KCl in deionized water or a combination of all three salts were then flowed through the cell at a rate of 20 mL/min as sketched in Figure 1. Digital photographs of the cell components are shown in Figure S1.

An additional experiment involved an FPW sample acquired from West Texas. The sample was recovered from well 9 (as referenced in our previous work) from Southern Midland in the Permian Basin of West Texas.[14] Access to FPW was enabled by University Lands, which maintains stewardship of the reservoir. The sample was filtered using a composite calcium sulfoaluminate (CSA)/glass-bead-coated stainless steel mesh membrane; deoiling and desilting were enabled by the orthogonal wettability imbued by ettringite needles formed in situ on the steel meshes upon hydration of CSA.[14] The membrane was incorporated within a MemXcell (model: MX-1-SS, Molecule Works Inc.) stainless-steel filtration cell. The FPW was filtered through the membrane using a peristaltic pump (Masterflex L/S Digital Drive with Easy-Load II Pump Head, 600 RPM, Cole-Parmer). The deoiled and desilted permeate was then diluted to 10% of its initial concentration using deionized water (Barnstead International NANOpure Diamond system ρ = 18.2 MΩ·cm). The conductivity of the input solution was in the range of 4−5 mS/cm.

The HCDI cell was connected to a Gamry Interface 1010E potentiostat in the repeating chronoamperometry mode. A voltage of 1.2 V was applied to the cell for time periods of 15, 30 min, 1, and 2 h at which point the potential was reversed to −1.2 V, for the same period of time, for a total of 40 cycles. The change in conductivity was measured using a combination of an ET915 conductivity electrode and EPU357 conductivity isopod and was plotted as a function of time.

Ion removal capacity was calculated by first plotting a calibration curve for each aqueous salt solution by recording the change in ionic conductivity as a function of the salt concentration. The change in conductivity after an ion removal step was converted to the concentration using the calibration curve and averaged across each measurement. The first few cycles correspond to conditioning steps. The ion removal capacity was then calculated using eq 1 where C_0 and C_i are the salt concentration before and after cycling, respectively; V is the solution volume; and M_{tot} is the mass of both electrodes including the active material and the carbon black and binder material.

$$\text{Ion removal capacity}\left(\frac{\text{mg}}{\text{g}}\right) = \frac{(C_0 - C_i \times V)}{M_{tot}} \quad (1)$$

Characterization. Powder X-ray diffraction (XRD) was performed on cycled positive electrode samples using a Bruker-AXS D8 Endeavor powder X-ray diffractometer equipped with a Lynxeye PSD XTE detector and a copper Kα source (λ = 1.5418 Å). A Pawley refinement was performed on the collected diffraction patterns.

X-ray photoelectron spectroscopy (XPS) experiments were conducted using Mg Kα X-rays (source energy of 1253.6 eV) in an Omicron DAR 400 XPS/UPS system equipped with a 128-channel micro-channel plate Argus detector and a CN10 electron flood source to neutralize sample charge. The instrumental energy resolution was approximately 0.8 eV. High-resolution fine spectra composited from triplicate acquisitions were collected at a pass energy of 100 eV (in the constant analyzer energy mode), with an energy step size of 0.05 eV and with a dwell time of 200 ms. All high-resolution spectra were calibrated using the C 1s line of adventitious carbon at 284.5 eV. Spectral line-shape fitting was performed with CasaXPS 2.3.16 software applying the Marquardt−Levenberg optimization algorithm.

Inductively coupled plasma mass spectrometry (ICP−MS) was performed on cycled positive electrode samples and used to determine the raw analyte concentration of V^{51}, Li^7, Na^{23}, and K^{39} using a PerkinElmer NExION300D instrument benchmarked to a Sc^{45} internal standard. Samples were prepared for ICP−MS analyses by removing the electrode material after an ion uptake cycle and washing 3× with 50 mL of deionized water (Barnstead International NANOpure Diamond system ρ = 18.2 MΩ·cm) in order to remove surface-adhered ions. The washed electrodes were then dried under nitrogen on a Schlenk line and digested in concentrated nitric acid at 100 °C in a water bath in a sealed centrifuge tube. The solution was then diluted with Milli-Q-purified H_2O until the estimated concentration of ions was in the 1−100 ppb range. The measured concentration of metal ions has a relative uncertainty of 5%.

https://doi.org/10.1021/acsami.2c17800
ACS Appl. Mater. Interfaces 2023, 15, 1554−1562

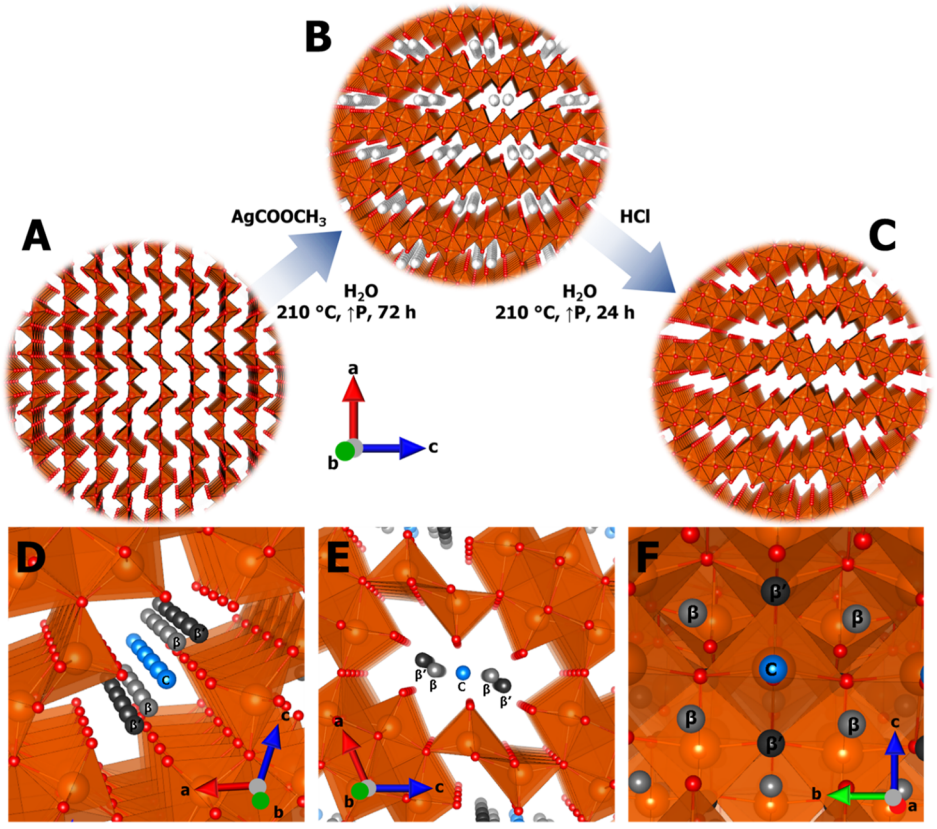

Figure 2. (A–C) Synthetic pathway and interstitial sites in ζ-V_2O_5. The schematic illustration of stabilization of metastable ζ-V_2O_5 based on topochemical de-intercalation of Ag ions from β-$Ag_{0.33}V_2O_5$. The crystal structures of the (A) α-V_2O_5, (B) β-$Ag_{0.33}V_2O_5$, and (C) ζ-V_2O_5 product are shown. (D–F) Illustration of the 1D tunnels of ζ-V_2O_5 along different axes depicting the range of accessible interstitial sites. β sites (multiplicity of 4 per unit cell) are shown as silver spheres, β' sites (multiplicity of 4 per unit cell) as black spheres, and C sites (multiplicity of 2 per unit cell) as blue spheres.

RESULTS AND DISCUSSION

Practical electrochemical desalination of FPW and brackish water streams requires fulfillment of a number of key performance constraints. First, the process must provide a high intrinsic reaction coordinate (IRC), and the active materials must remain insoluble even when subject to modest pH excursions. Next, the sequestration of ions from flow streams must be entirely reversible so that the ions can be released in the form of concentrated brine streams, and the cell can be continuously cycled. Third, the feasibility of a CDI process would be greatly enhanced if ion sequestration can be accomplished with some degree of selectivity, such as to enable selective capture of high-value ions. We will demonstrate below that these constraints can be satisfied by the use of the HCDI cell with ζ-V_2O_5 positive electrodes.

ζ-V_2O_5 has attracted substantial recent attention as a battery positive electrode material owing to its high theoretical capacity (441 mA h/g), outstanding thermal and chemical stability, ability to accommodate Li and Mg ions through reordering of cation occupancies but without distortive phase transitions, low stress accumulation upon cation insertion, and excellent cyclability.[20,30] The ζ-V_2O_5 polymorph comprises three crystallographically distinct vanadium centers, specifically two distorted VO_6 octahedra interwoven by VO_5 square pyramids, which define a 1D tunnel oriented along the *b*-axis.[30] Figure 2A–C shows the sequence of reactions used to stabilize ζ-V_2O_5. β-$Ag_{0.33}V_2O_5$ nanowires are prepared by the reaction of silver acetate with α-V_2O_5; topochemical deinsertion of Ag^+ ions by treatment with HCl yields the ζ-V_2O_5 polymorph. Figure S2 shows a refined XRD pattern of ζ-V_2O_5 nanowires. ζ-V_2O has multiple interstitial sites—β, β', and C—arrayed along the 1D tunnel, as shown in Figure 2D–F, with site multiplicities of 4, 4, and 2, respectively.[19,30,34,35] The prepared nanowires are crystallized in a monoclinic $C2/m$ space group with a β-angle of 110.0°. Figure S3 shows scanning electron microscopy (SEM) and transmission electron microscopy (TEM) images of the ζ-V_2O_5 nanowires. The nanowires have approximately rectangular cross-sections with dimensions of 0.33 ± 0.09 μm and range in length from 0.5 to 9 μm.

In order to demonstrate the viability of ζ-V_2O_5 as a positive electrode for HCDI, we compare a flow cell with a ζ-V_2O_5 positive electrode and activated carbon negative electrode with a conventional CDI cell with an identical activated carbon negative electrode and positive electrode pair. The electrodes are prepared with the same specifications and used within the same exact flow cell varying just the active electrode material.

Aqueous solutions of 15.04 mm NaCl, KCl, and LiCl have been used as the input flow streams. A constant potential is applied for varying time periods. In addition to these test streams, we have examined (a) a mixed-salt aqueous solution with 5 mM each of NaCl, KCl, and LiCl and (b) a realistic FPW flow stream from the Permian Basin.

Figure 3 contrasts cycling data for K-ion removal at a constant potential of 1.2 V for CDI and HCDI cells where the solution is flowed at a rate of 20 mL/min. The CDI cells comprising activated carbon active electrodes rapidly reach

https://doi.org/10.1021/acsami.2c17800
ACS Appl. Mater. Interfaces 2023, 15, 1554–1562

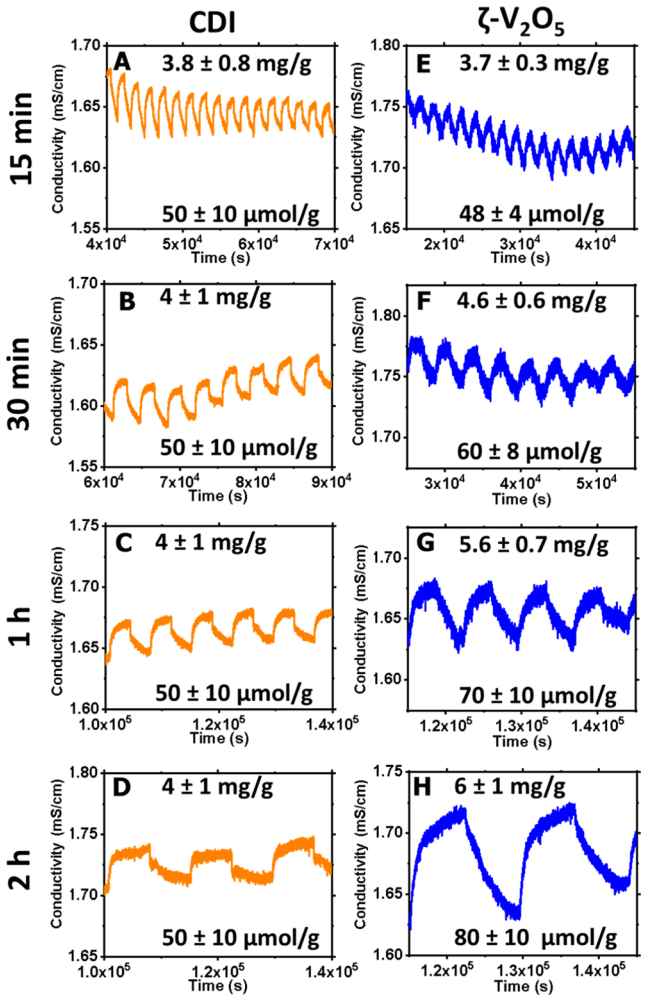

Figure 3. Cycling experiments for CDI cells (A−D) and HCDI cells (E−H). An aqueous solution of 15.04 mm KCl pumped at a constant flow rate of 20 mL/min. The cells were cycled at 1.2 V for times varying from 15 min to 2 h, and then, the potential was reversed to −1.2 V. The cells were cycled a total of 40 times. Data is plotted as the conductivity of the solution vs time. The average IRC across the cycles is inset into each plot.

their maximum ion removal capacity, peaking at a cycle time of 30 min, which reflects the limits of ions that can be sequestered at the surfaces of the electrodes. In contrast, HCDI cells show characteristic signs of time-dependent ion removal, arising from kinetics of pseudocapacitive surface Faradaic reactions and diffusion limitations from propagation of an intercalation wave, reaching an IRC of 6 mg/g as a function of total electrode mass or 18 mg/g as a function of the ζ-V_2O_5 positive electrode material, a 50% increase as compared to the CDI system after 2 h.[36] Figures S4 and S5 contrast the IRC of CDI and HCDI configurations (the latter with ζ-V_2O_5 positive electrodes) toward aqueous solutions of Na^+ and Li^+; a 16 and 50% increase is observed in the IRC for ζ-V_2O_5 insertion as compared to non-specific capacitive removal, respectively. Figure 4 and Table S1 summarize the results for the three test aqueous solutions. The HCDI values correspond to both Faradaic pseudocapacitive and insertion processes—which are further differentiated based on characterization of the recovered materials. The improvements in the IRC observed as a result of the operation of Faradaic pseudocapacitive and intercalative processes point to the promise of thick electrodes

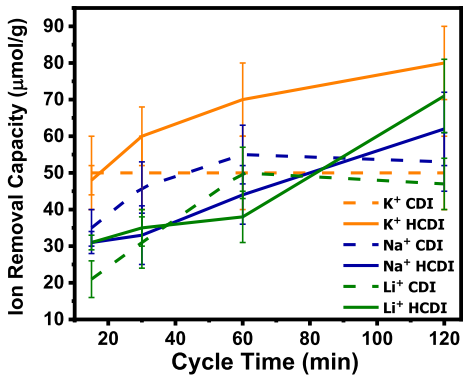

Figure 4. Ion removal capacity for CDI and HCDI configurations for Li, Na, and K ions. The IRC as a function of total electrode mass contrasting the performance of the CDI and HCDI system for input flow streams of 15.04 mm aqueous solutions of KCl, NaCl, and LiCl flowed at a rate of 20 mL/min. The horizontal axis represents the half-cycle time for each sample. Each value for the IRC is represented in μmol of salt removed per gram of the electrode.

to engender further increases in single-cycle ion removal. As will be further discussed below, the viability of bulk intercalation in ζ-V_2O_5 paves the way to implementing lessons learned from high-energy-density battery electrode architectures with appropriate tortuosity of ion transport pathways to allow electrolyte permeation and effective utilization of the active material.[37,38]

Several trends are immediately discernible from Figure 4 and Table S1. The kinetics of ion sequestration in CDI using activated carbon electrodes is relatively faster for K ions; saturation is reached in 30 min, but ca. 1 h is required for saturation of the activated carbon surfaces with Na and Li ions. This is consistent with the higher ionic conductivity of KCl aqueous solutions, concordant with the relatively smaller size of hydrated K ions.[39] In contrast, for HCDI with ζ-V_2O_5 active electrodes, relatively slower uptake is observed, which is attributable to the kinetics of Faradaic reactions at surfaces and solid-state diffusion through the 1D tunnels after desolvation at the charged interface.

Potassium uptake in ζ-V_2O_5 surpasses that of the CDI system at a 30 min half-cycle time, whereas a 2 h half-cycle time is needed for Li-ion insertion in ζ-V_2O_5 to surpass capacitive adsorption on activated carbon. This can be rationalized based on the hydration free energy differences between K^+ and Li^+ in aqueous media (271−343 and 515−544 kJ/mol, respectively).[40] The higher hydrated ionic radius and greater hydration free energy pose a greater barrier to interfacial desolvation, suggesting a higher selectivity for K^+ at shorter cycle times. However, the maximum IRC as a function of the total electrode mass in moles after 2 h for HCDI is K (80 μmol/g), Na (62 μmol/g), and Li (71 μmol/g) (Figure 4 and Table S1) or 242, 185, and 213 μmol/g, respectively, as a function of the ζ-V_2O_5 positive electrode material, which indicates a balance between ionic and solvated radii of the ions and furthermore parallels the ordering of site-to-site migration barriers and solid-state diffusion coefficients for the three ions.[34,41] Although K has a smaller dehydration barrier and is much more rapidly able to desolvate and participate in surface Faradaic processes and/or diffuse into the tunnels of ζ-V_2O_5 upon intercalation, fewer sites are available for potassium and sodium, and migration barriers for these ions are relatively larger, thus suggesting the potential for

https://doi.org/10.1021/acsami.2c17800
ACS Appl. Mater. Interfaces 2023, 15, 1554−1562

greater lithium intercalation in a mixed stream or at extended cycle times.

ICP−MS has been performed on ζ-V_2O_5 electrodes recovered after discharge; the recovered material is washed three times with deionized water to remove surface-bound ions. Based on the ICP−MS measurements, stoichiometries of 0.66 Li, 0.18 Na, and 0.07 K per V_2O_5 formula unit are inferred, which suggests the potential for greater selectivity toward sequestration of Li ions at longer cycle times, which is again consistent with the ordering of solid-state diffusion coefficients of the three ions in ζ-V_2O_5.[34,41] Density functional theory simulations have shown that barriers to Li-ion diffusion are 0.13−0.14 in ζ-V_2O_5 depending on the Li-ion stoichiometry; activation energies for Na-ion diffusion are substantially higher at 0.47−0.95 eV.[34,42] Although the activation energy for K-ion diffusion in ζ-V_2O_5 has not been calculated, it is expected to be much higher than that for Na^+ given the constrained trigonal planar transition state for ion migration between β/β' sites,[31,34] which falls directly into the observed trend based on the ionic radii. As such, while K-ion removal is mediated by Faradaic processes, pseudocapacitive rather than insertion processes dominate for the larger ion.

XPS data has furthermore been acquired for recovered electrodes after ion sequestration cycles and washing with deionized water to remove adsorbed ions (Figures S6 and S7).[43,44] Li 1s, Na 1s, and K 2p peaks are observed at 56, 1070, and 292 eV, respectively, corroborating the presence of the intercalated ions. The as-prepared ζ-V_2O_5 positive electrode material showed vanadium and oxygen manifolds centered at binding energies of 517 and 530 eV, respectively. Upon lithiation, a low-energy shoulder increases for the V $2p_{3/2}$ peaks corresponding to vanadium reduction (Figures S6 and S7).[30] The observed reduction of V to its tetravalent form indicates intercalation of ions to form β-$M_xV_2O_5$, which evidences Faradaic processes and redox intercalation of ions within the 1D tunnels of ζ-V_2O_5. A low-energy shoulder to the V $2p_{3/2}$ peak is likewise observed in the β-$K_xV_2O_5$ material with a lesser degree of reduction for β-$Na_xV_2O_5$.

XPS is exceedingly surface-sensitive, and thus, to obtain definitive evidence for ion intercalation (and not just surface pseudocapacitive processes), we have performed powder XRD measurements on recovered ζ-V_2O_5 electrodes after ion sequestration cycles. Figure 5 contrasts powder XRD patterns acquired for samples after HCDI removal of Li, Na, and K ions with the XRD pattern of as-prepared ζ-V_2O_5. Pawley refinements have been performed using the powder XRD data; the refined lattice parameters are listed in Table 1. The recovered samples are still crystallized in the monoclinic structure with a $C2/m$ space group. However, a substantial volume expansion of 1.9, 1.2, and 0.4% is observed upon K^+, Li^+, and Na^+ insertion, respectively (Table 1). The observed changes in lattice parameters and expansion of the unit cell are consistent with the intercalation stoichiometries derived from ICP−MS noted in Table 1. Similar lattice expansion has been observed for non-aqueous intercalation in ζ-V_2O_5 single crystals, corroborating the occupancy of interstitial sites within the tunnel and the operation of Faradaic reactions at the charged interfaces of the HCDI cell.[30]

Notably, below a threshold stoichiometry of $x \approx 0.33$ in $Li_xV_2O_5$, inserted Li ions initially occupy five-coordinated β-sites (Figure 2D−F) within the V_2O_5 tunnels, which engenders only modest distortion of the lattice; however, as the Li occupancy increases, cation reordering is observed, accompanied by tunnel expansion, and the Li ions are arrayed along more closely spaced four-coordinated β' sites (Figure 2D−F).[41] This allows for a Li-ion stoichiometry of up to $x \sim 0.67$. However, Na^+ and K^+ ions cannot be accommodated within β'-sites and are accommodated up to maximum stoichiometries of ∼0.33 per formula unit, being confined to the β-sites shown in Figure 2D−F.

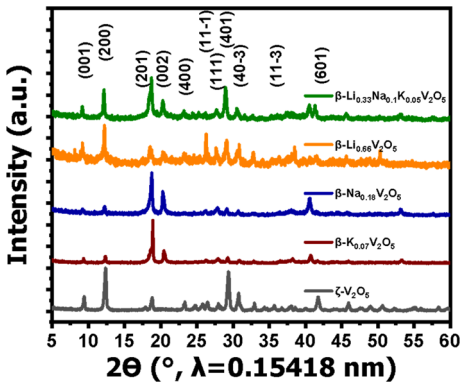

Figure 5. Evidence of interstitial site filling from powder XRD. XRD data for an uncycled ζ-V_2O_5 electrode and electrodes cycled with 15.04 mm solutions of KCl (red), NaCl (blue), and LiCl (orange) and a solution containing 5.01 mm KCl, 5.01 mm NaCl, and 5.01 mm LiCl (green) in deionized water. The labels to each XRD pattern denote stoichiometries measured by ICP−MS.

We next examine competitive sequestration from a mixed-salt stream. Figure 6A shows the electrochemical performance of HCDI cells with ζ-V_2O_5 positive electrodes in the removal of cations from a mixed aqueous solution of LiCl, NaCl, and KCl at different half-cycle times at a flow rate of 20 mL/min and an applied potential of 1.2 V. ICP−MS results in Table 1 illustrate a strong preference for Li-ion insertion after 2 h; Li ions are 33% of the cations in solution but represent 68% of the intercalated ions (Table 1), illustrating a means of selective sequestration. This is further corroborated by the XPS results shown in Figures S6 and S7. The high-resolution V 2p XPS spectra in Figures S6 and S7 show a clear shoulder between 515 and 516 eV indicating the presence of tetravalent vanadium, which is suggestive of significant ion intercalation.[41] Powder XRD results in Figure 5 further demonstrate a 1.3% lattice expansion of ζ-V_2O_5 upon insertion of ions from the mixed-salt flow stream. The results thus demonstrate that the kinetics of HCDI using ζ-V_2O_5 electrodes are dependent to a large extent on the hydrated ion size and hydration energy; a lower hydration energy is conducive to higher ionic conductivity and easier desolvation at interfaces of insertion electrodes. However, the IRC at extended times, when desolvation is no longer the limiting process, is proportional to the availability of interstitial sites and the site-to-site migration barriers of bare ions. The results provide unequivocal evidence for intercalative cation sequestration and suggest a means of engendering ion selectivity.

In an attempt to evidence the real-world potential of a ζ-V_2O_5 positive electrode material for desalination and selective ion sequestration in an HCDI configuration, FPW samples from a hydraulic fracturing operation located in the Southern Permian Basin in West Texas were flowed through the flow cell configuration depicted in Figure 1 after being filtered for residual oil and dissolved solids using a novel CSA/glass-bead-coated stainless steel mesh membrane.[14] The resulting aqueous solution has an extremely high salt content, which necessitates

https://doi.org/10.1021/acsami.2c17800
ACS Appl. Mater. Interfaces 2023, 15, 1554−1562

Table 1. ICP−MS Results and Unit-Cell Parameters Derived from a Pawley Refinement for Positive Electrode Materials That Have Been Cycled with 15.04 mm LiCl, 15.04 mm NaCl, 15.04 mm KCl, and a Mixed-Salt Solution Containing 5.01 mm LiCl, 5.01 mm NaCl, and 5.01 mm KCl

ICP−MS	a (Å)	b (Å)	c (Å)	β-angle (°)	unit-cell volume (Å^3)	expansion (%)
ζ-V_2O_5	15.31	3.6	10.07	109.8	522.6	0.0
β'-$Li_{0.66}V_2O_5$	15.19	3.63	10.07	108	528.9	1.2
β-$Na_{0.18}V_2O_5$	15.19	3.63	10.04	108.3	524.9	0.4
β-$K_{0.07}V_2O_5$	15.25	3.63	10.09	107.8	532.4	1.9
β-$Li_{0.33}Na_{0.1}K_{0.05}V_2O_5$	15.23	3.63	10.06	108.15	529.2	1.3

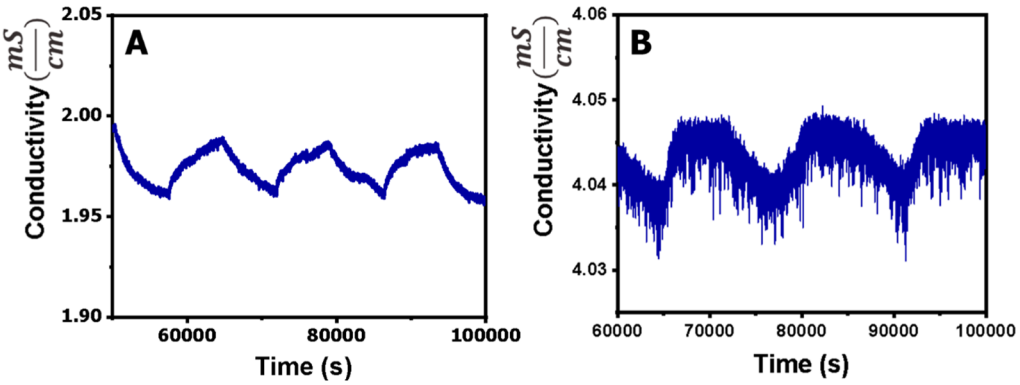

Figure 6. (A) Desalination of a mixed-salt solution. Electrochemical cycling results for an HCDI cell with an aqueous solution of 5 mM LiCl, 5 mM NaCl, and 5 mM KCl flowed at a constant flow rate of 20 mL/min. The cell was cycled at 1.2 V for 2 h, and then, the potential was reversed to −1.2 V. The cell was cycled a total of 40 times. Data is plotted as the conductivity of the solution vs time. (B) Desalination of the produced water stream. Cycling experiment for an HCDI cell with a 10 vol. % solution of FPW from a hydraulic fracturing operation in West Texas. The water was first filtered to remove residual oil and dissolved solids using a CSA/glass-bead/stainless-steel-mesh-based membrane and then flowed at a constant flow rate of 20 mL/min.[14] The cell was cycled at 1.2 V for 2 h, and then, the potential was reversed to −1.2 V. The cell was cycled a total of 40 times. Data is plotted as the conductivity of the solution vs time.

dilution of the sample to 10% of its initial concentration prior to desalination. Although the pretreatment using the cement-based membranes removed the majority of residual silt and oil, additional pretreatment of the FPW can be further performed as part of a treatment train. Suspended solids and total dissolved solids have been removed from similar FPW samples through the use of coagulation, flocculation, and sedimentation techniques, which provide an alternative to dilution.[45] The salt content of the FPW was measured by ICP−MS (Table 2). A

Table 2. ICP−MS Results of the Ionic Composition of Residual Salt upon Evaporation of FPW[a]

	Li	Na	K	Mg	Ca	Sr
salt composition (at. %)	0.35	94.03	0.95	1.02	3.25	0.40
sequestered ions (at. %)	7.29	24.27	20.38	13.66	33.38	1.01

[a]The water was first filtered to remove residual oil and dissolved solids using a cement-based membrane, and then, salt was recovered through evaporation of the aqueous phase. These results are contrasted with ICP−MS results of the intercalated ion content of a ζ-V_2O_5 positive electrode after flowing an FPW stream as shown in Figure 3.

diluted sample cycled through the HCDI cell shows effective removal of ionic impurities (Figure 6B). Although evidence of sequestration in the porous ζ-V_2O_5 electrode is observed for each of the ions identified in the initial solution, the ICP−MS results in Table 2 provide evidence for selective sequestration of Li ions.

Although the pH of this FPW is nearly neutral (ca. pH 6.62), anticipated increases in atmospheric acidification could lead to lower-pH operating conditions in the near future. In an attempt to demonstrate the stability of the electrode material under acidic conditions, samples of the active material were immersed in pH 6.20 and pH 5.35 aqueous solutions of HCl for 7 days. Powder XRD patterns of the recovered material showed no indications of degradation, demonstrating stability of the material even under acidic conditions (Figure S8). The results demonstrate clear evidence of the viability of ζ-V_2O_5 as a positive electrode material for effective desalination and Li-ion extraction from FPW.

CONCLUSIONS

We demonstrate that a tunnel-structured ζ-V_2O_5 insertion host serves as an effective positive electrode material for desalination of aqueous salt solutions in an HCDI configuration. Ion removal experiments were performed at varying half-cycle times with aqueous solutions containing Li^+, Na^+, K^+, a mixed-salt solution containing all three ions, and a filtered FPW stream from the Permian Basin. The HCDI cell demonstrates ca. 50% superior Li^+ and K^+ removal from aqueous flow streams and ca. 16% improvement in the IRC for Na^+ as compared to CDI cells built according to the same specifications deployed within an identical cell architecture. ICP−MS and XPS data corroborate ion sequestration within the active ζ-V_2O_5 electrodes; the latter points to the reduction of vanadium, suggesting the operation of Faradaic surface pseudocapacitive and redox intercalation processes. Pawley refinements to powder XRD data unambiguously establish that ion sequestration occurs through ion insertion in the interstitial

https://doi.org/10.1021/acsami.2c17800
ACS Appl. Mater. Interfaces 2023, 15, 1554−1562

sites of the 1D tunnel of ζ-V_2O_5. The kinetics of ion removal show considerable dependence on the free energy of hydration, which governs the ease of desolvation at the electrode/electrolyte interface. At longer time periods, the IRC is a function primarily of the ionic radius of the bare ion and its solid-state diffusion coefficient. ζ-V_2O_5 positive electrodes show substantial selectivity for Li^+ removal from mixed-ion flow streams and enrichment of the Li-ion concentration from FPW. Future work will focus on optimization of the porous electrode architecture and cell geometry to allow for a higher IRC and pre-intercalation to achieve improved selectivity. HCDI thus shows promise not only for clean FPW but also to extract valuable minerals needed for the energy transition.

■ ASSOCIATED CONTENT

Supporting Information

The Supporting Information is available free of charge at https://pubs.acs.org/doi/10.1021/acsami.2c17800.

Photographs of individual components of the HCDI cell; Rietveld refinement of the ζ-V_2O_5 positive electrode material; SEM and TEM images; additional cycling experiments with Na ions; additional cycling experiments with Li ions; IRC data; XPS results of the cycling experiments; XPS results of mixed ion solutions; and acid-stability study (PDF)

■ AUTHOR INFORMATION

Corresponding Author

Sarbajit Banerjee − *Department of Chemistry and Department of Materials Science and Engineering, Texas A&M University, College Station, Texas 77843-3012, United States;* orcid.org/0000-0002-2028-4675; Email: banerjee@chem.tamu.edu

Authors

Nicholas I. Cool − *Department of Chemistry and Department of Materials Science and Engineering, Texas A&M University, College Station, Texas 77843-3012, United States*

Randall James − *Department of Chemistry, Texas A&M University, College Station, Texas 77843-3012, United States*

Parker Schofield − *Department of Chemistry and Department of Materials Science and Engineering, Texas A&M University, College Station, Texas 77843-3012, United States*

Joseph V. Handy − *Department of Chemistry and Department of Materials Science and Engineering, Texas A&M University, College Station, Texas 77843-3012, United States*

Mukul Bhatia − *Department of Geology and Geophysics, Texas A&M University, College Station, Texas 77843-3012, United States*

Complete contact information is available at: https://pubs.acs.org/10.1021/acsami.2c17800

Notes

The authors declare no competing financial interest.

■ ACKNOWLEDGMENTS

This project was supported by University Lands and by the National Science Foundation under DMR 1809866. N.I.C. acknowledges the support of the NSF under a Graduate Research Fellowship grant DGE: 1746932. SEM and EDS were performed in the Texas A&M University Materials Characterization Core Facility (RRID:SCR_022202). Use of the TAMU Microscopy and Imaging Center is acknowledged.

■ REFERENCES

(1) Mekonnen, M. M.; Hoekstra, A. Y. Four Billion People Facing Severe Water Scarcity. *Sci. Adv.* **2016**, *2*, No. e1500323.

(2) Chang, H.; Li, T.; Liu, B.; Vidic, R. D.; Elimelech, M.; Crittenden, J. C. Potential and Implemented Membrane-Based Technologies for the Treatment and Reuse of Flowback and Produced Water from Shale Gas and Oil Plays: A Review. *Desalination* **2019**, *455*, 34−57.

(3) Zhang, Y.; Mao, J.; Mao, J.; Chen, A.; Yang, X.; Lin, C.; Wei, Z.; Huang, X.; Song, L.; Tang, F.; Jiang, Q.; Ni, Y. Towards Sustainable Oil/Gas Fracking by Reusing its Process Water: A Review on Fundamentals, Challenges, and Opportunities. *J. Petrol. Sci. Eng.* **2022**, *213*, 110422.

(4) Alabi, A.; AlHajaj, A.; Cseri, L.; Szekely, G.; Budd, P.; Zou, L. Review of Nanomaterials-Assisted Ion Exchange Membranes for Electromembrane Desalination. *npj Clean Water* **2018**, *1*, 10.

(5) Abraham, J.; Vasu, K. S.; Williams, C. D.; Gopinadhan, K.; Su, Y.; Cherian, C. T.; Dix, J.; Prestat, E.; Haigh, S. J.; Grigorieva, I. V.; Carbone, P.; Geim, A. K.; Nair, R. R. Tunable Sieving of Ions Using Graphene Oxide Membranes. *Nat. Nanotechnol.* **2017**, *12*, 546−550.

(6) Gamaethiralalage, J. G.; Singh, K.; Sahin, S.; Yoon, J.; Elimelech, M.; Suss, M. E.; Liang, P.; Biesheuvel, P. M.; Zornitta, R. L.; de Smet, L. C. P. M. Recent Advances in Ion Selectivity with Capacitive Deionization. *Energy Environ. Sci.* **2021**, *14*, 1095−1120.

(7) Manchanda, H.; Kumar, M. Study of Water Desalination Techniques and a Review on Active Solar Distillation Methods. *Environ. Prog. Sustainable Energy* **2018**, *37*, 444−464.

(8) Di Vincenzo, M.; Tiraferri, A.; Musteata, V.-E.; Chisca, S.; Sougrat, R.; Huang, L.-B.; Nunes, S. P.; Barboiu, M. Biomimetic Artificial Water Channel Membranes for Enhanced Desalination. *Nat. Nanotechnol.* **2021**, *16*, 190−196.

(9) Guo, J.; Tucker, Z. D.; Wang, Y.; Ashfeld, B. L.; Luo, T. Ionic Liquid Enables Highly Efficient Low Temperature Desalination by Directional Solvent Extraction. *Nat. Commun.* **2021**, *12*, 437.

(10) Tian, L.; Chang, H.; Tang, P.; Li, T.; Zhang, X.; Liu, S.; He, Q.; Wang, T.; Yang, J.; Bai, Y.; Vidic, R. D.; Crittenden, J. C.; Liu, B. Rare Earth Elements Occurrence and Economical Recovery Strategy from Shale Gas Wastewater in the Sichuan Basin, China. *ACS Sustainable Chem. Eng.* **2020**, *8*, 11914−11920.

(11) Liu, C.; Hsu, P.-C.; Xie, J.; Zhao, J.; Wu, T.; Wang, H.; Liu, W.; Zhang, J.; Chu, S.; Cui, Y. A Half-Wave Rectified Alternating Current Electrochemical Method for Uranium Extraction from Seawater. *Nat. Energy* **2017**, *2*, 17007.

(12) Wang, Z.; Meng, Q.; Ma, R.; Wang, Z.; Yang, Y.; Sha, H.; Ma, X.; Ruan, X.; Zou, X.; Yuan, Y.; Zhu, G. Constructing an Ion Pathway for Uranium Extraction from Seawater. *Chem* **2020**, *6*, 1683−1691.

(13) Scanlon, B. R.; Ikonnikova, S.; Yang, Q.; Reedy, R. C. Will Water Issues Constrain Oil and Gas Production in the United States? *Environ. Sci. Technol.* **2020**, *54*, 3510−3519.

(14) Rivera-Gonzalez, N.; Bajpayee, A.; Nielsen, J.; Zakira, U.; Zaheer, W.; Handy, J.; Sill, T.; Birgisson, B.; Bhatia, M.; Banerjee, S. Textured Ceramic Membranes for Desilting and Deoiling of Produced Water in the Permian Basin. *iScience* **2022**, *25*, 105063.

(15) Lee, J.; Kim, S.; Kim, C.; Yoon, J. Hybrid Capacitive Deionization to Enhance the Desalination Performance of Capacitive Techniques. *Energy Environ. Sci.* **2014**, *7*, 3683−3689.

(16) Wu, T.; Wang, G.; Wang, S.; Zhan, F.; Fu, Y.; Qiao, H.; Qiu, J. Highly Stable Hybrid Capacitive Deionization with a MnO2 Anode and a Positively Charged Cathode. *Environ. Sci. Technol. Lett.* **2018**, *5*, 98−102.

(17) Siekierka, A.; Tomaszewska, B.; Bryjak, M. Lithium Capturing from Geothermal Water by Hybrid Capacitive Deionization. *Desalination* **2018**, *436*, 8−14.

(18) Bardi, U. Extracting Minerals from Seawater: an Energy Analysis. *Sustainability* **2010**, *2*, 980−992.

(19) Marley, P. M.; Abtew, T. A.; Farley, K. E.; Horrocks, G. A.; Dennis, R. V.; Zhang, P.; Banerjee, S. Emptying and Filling a Tunnel Bronze. *Chem. Sci.* **2015**, *6*, 1712−1718.
(20) Luo, Y.; Rezaei, S.; Santos, D. A.; Zhang, Y.; Handy, J. V.; Carrillo, L.; Schultz, B. J.; Gobbato, L.; Pupucevski, M.; Wiaderek, K.; Charalambous, H.; Yakovenko, A.; Pharr, M.; Xu, B.-X.; Banerjee, S. Cation Reordering Instead of Phase Transitions: Origins and Implications of Contrasting Lithiation Mechanisms in 1D ζ- and 2D α-V_2O_5. *Proc. Natl. Acad. Sci. U.S.A.* **2022**, *119*, No. e2115072119.
(21) Anderson, M. A.; Cudero, A. L.; Palma, J. Capacitive Deionization as an Electrochemical means of Saving Energy and Delivering Clean Water. Comparison to Present Desalination Practices: Will it Compete? *Electrochim. Acta* **2010**, *55*, 3845−3856.
(22) Porada, S.; Zhao, R.; van der Wal, A.; Presser, V.; Biesheuvel, P. M. Review on the Science and Technology of Water Desalination by Capacitive Deionization. *Prog. Mater. Sci.* **2013**, *58*, 1388−1442.
(23) Folaranmi, G.; Bechelany, M.; Sistat, P.; Cretin, M.; Zaviska, F. Towards Electrochemical Water Desalination Techniques: A Review on Capacitive Deionization, Membrane Capacitive Deionization and Flow Capacitive Deionization. *Membranes* **2020**, *10*, 96.
(24) Byles, B. W.; Hayes-Oberst, B.; Pomerantseva, E. Ion Removal Performance, Structural/Compositional Dynamics, and Electrochemical Stability of Layered Manganese Oxide Electrodes in Hybrid Capacitive Deionization. *ACS Appl. Mater. Interfaces* **2018**, *10*, 32313−32322.
(25) Kim, S.; Lee, J.; Kim, C.; Yoon, J. Na2FeP2O7 as a Novel Material for Hybrid Capacitive Deionization. *Electrochim. Acta* **2016**, *203*, 265−271.
(26) Byles, B. W.; Cullen, D. A.; More, K. L.; Pomerantseva, E. Tunnel Structured Manganese Oxide Nanowires as Redox Active Electrodes for Hybrid Capacitive Deionization. *Nano Energy* **2018**, *44*, 476−488.
(27) Porada, S.; Borchardt, L.; Oschatz, M.; Bryjak, M.; Atchison, J.; Keesman, K.; Kaskel, S.; Biesheuvel, P.; Presser, V. Direct Prediction of the Desalination Performance of Porous Carbon Electrodes for Capacitive Deionization. *Energy Environ. Sci.* **2013**, *6*, 3700−3712.
(28) Kumar, A.; Fukuda, H.; Hatton, T. A.; Lienhard, J. H. Lithium Recovery from Oil and Gas Produced Water: A Need for a Growing Energy Industry. *ACS Energy Lett.* **2019**, *4*, 1471−1474.
(29) Whittingham, M. S. Lithium Batteries: 50 Years of Advances to Address the Next 20 Years of Climate Issues. *Nano Lett.* **2020**, *20*, 8435−8437.
(30) Handy, J. V.; Luo, Y.; Andrews, J. L.; Bhuvanesh, N.; Banerjee, S. An Atomic View of Cation Diffusion Pathways from Single-Crystal Topochemical Transformations. *Angew. Chem., Int. Ed.* **2020**, *59*, 16385−16392.
(31) De Jesus, L. R.; Andrews, J. L.; Parija, A.; Banerjee, S. Defining Diffusion Pathways in Intercalation Cathode Materials: Some Lessons from V_2O_5 on Directing Cation Traffic. *ACS Energy Lett.* **2018**, *3*, 915−931.
(32) Santos, D. A.; Dixit, M. K.; Pradeep Kumar, P.; Banerjee, S. Assessing the Role of Vanadium Technologies in Decarbonizing Hard-to-Abate Sectors and Enabling the Energy Transition. *iScience* **2021**, *24*, 103277.
(33) Santos, D. A.; Pradeep Kumar, P.; Dixit, M. K.; Banerjee, S. Building Back Better: Lessons Learned from Sichuan Earthquake on Decarbonizing China's Construction Industry through Microalloying. *Matter* **2021**, *4*, 4−9.
(34) Parija, A.; Liang, Y.; Andrews, J. L.; De Jesus, L. R.; Prendergas, D.; Banerjee, S. Topochemically De-Intercalated Phases of V_2O_5 as Cathode Materials for Multivalent Intercalation Batteries: A First-Principles Evaluation. *Chem. Mater.* **2016**, *28*, 5611−5620.
(35) Luo, Y.; Bai, Y.; Mistry, A.; Zhang, Y.; Zhao, D.; Sarkar, S.; Handy, J. V.; Rezaei, S.; Chuang, A. C.; Carrillo, L.; Wiaderek, K.; Pharr, M.; Xie, K.; Mukherjee, P. P.; Xu, B.-X.; Banerjee, S. Effect of Crystallite Geometries on Electrochemical Performance of Porous Intercalation Electrodes by Multiscale Operando Investigation. *Nat. Mater.* **2022**, *21*, 217−227.
(36) Fraggedakis, D.; Nadkarni, N.; Gao, T.; Zhou, T.; Zhang, Y.; Han, Y.; Stephens, R. M.; Shao-Horn, Y.; Bazant, M. Z. A Scaling Law to Determine Phase Morphologies During Ion Intercalation. *Energy Environ. Sci.* **2020**, *13*, 2142−2152.
(37) Singh, M.; Kaiser, J.; Hahn, H. Thick Electrodes for High Energy Lithium Ion Batteries. *J. Electrochem. Soc.* **2015**, *162*, A1196.
(38) Kuang, Y.; Chen, C.; Kirsch, D.; Hu, L. Thick Electrode Batteries: Principles, Opportunities, and Challenges. *Adv. Energy Mater.* **2019**, *9*, 1901457.
(39) Zhong, C.; Deng, Y.; Hu, W.; Qiao, J.; Zhang, L.; Zhang, J. A Review of Electrolyte Materials and Compositions for Electrochemical Supercapacitors. *Chem. Soc. Rev.* **2015**, *44*, 7484−7539.
(40) Tansel, B. Significance of Thermodynamic and Physical Characteristics on Permeation of Ions During Membrane Separation: Hydrated Radius, Hydration Free Energy and Viscous Effects. *Sep. Purif. Technol.* **2012**, *86*, 119−126.
(41) Horrocks, G. A.; Parija, A.; De Jesus, L. R.; Wangoh, L.; Sallis, S.; Luo, Y.; Andrews, J. L.; Jude, J.; Jaye, C.; Fischer, D. A.; Prendergast, D.; Piper, L. F. J.; Banerjee, S. Mitigating Cation Diffusion Limitations and Intercalation-Induced Framework Transitions in a 1D Tunnel-Structured Polymorph of V_2O_5. *Chem. Mater.* **2017**, *29*, 10386−10397.
(42) Shepard, R.; Smeu, M. Ab Initio Investigation of α- and ζ-V_2O_5 for Beyond Lithium Ion Battery Cathodes. *J. Power Sources* **2020**, *472*, 228096.
(43) Akashi, N.; Kuroda, S.-i. Protein Immobilization onto Poly (Vinylidene Fluoride) Microporous Membranes Activated by the Atmospheric Pressure Low Temperature Plasma. *Polymer* **2014**, *55*, 2780−2791.
(44) Chen, X.; Wang, X.; Fang, D. a Review on C1s XPS-Spectra for Some Kinds of Carbon Materials. *Fullerenes, Nanotubes, Carbon Nanostruct.* **2020**, *28*, 1048−1058.
(45) Kaishentayev, D.; Hascakir, B. Pretreatment of Produced Waters Containing High Total Dissolved Solids; *SPE Annual Technical Conference and Exhibition*; OnePetro, 2021.

https://doi.org/10.1021/acsami.2c17800
ACS Appl. Mater. Interfaces 2023, 15, 1554−1562